The High-Temperature Cu-Fe-S System: Thermodynamic Analysis and Prediction of the Liquid–Solid Phase Range

Peter Waldner[1]

Abstract Thermodynamic modeling of the Cu-Fe-S liquid solution is carried in the framework of the modified quasichemical model. The manifold nature of Cu-Fe-S liquid solutions from highly metallic via sulfur-rich to pure liquid sulfur is described by one single Gibbs energy expression at 1 bar total pressure. The model predictive ability of an asymmetric versus symmetric approach is thermodynamically analyzed with respect to the extrapolation scheme from the binary subsystems into the ternary system. Without the need of adjustable ternary parameters predictions of sulfur potentials for the liquid phase are in line with experimental data available in the literature. High-temperature pyrrhotite optimized via the compound energy formalism and Cu-Fe-S alloy phases are taken into consideration to predict phase equilibria with the liquid solution. Four isothermal and four isoplethal sections demonstrate promising agreement between a large stock of experimental data and prediction.

Keywords copper · copper-iron-sulfur system · iron · phase diagram · sulfur · thermodynamic modeling

1 Introduction

Due to the fundamental role of copper and iron in metallurgy and geochemistry extensive experimental and theoretical efforts were dedicated to the Cu-Fe-S system.

Especially in copper metallurgy, the high-temperature Cu-Fe-S system with its complex ternary liquid solution attracts much attention. The properties of the Cu-Fe-S liquid solution range from a metallic copper-rich melt over a so-called matte, the metallurgical notation for a sulfur-rich liquid phase, to pure liquid sulfur. Reflecting this peculiarity from a thermodynamic point of view, reliable model prediction of the Gibbs energy of the Cu-Fe-S liquid solution can support further progress on several levels of research.

Evaluation and compilation of thermodynamic and phase equilibria data from the literature for the Fe-Cu-S system were the focus of Chang et al.[1,2] Kongoli et al.[3] and Degterov and Pelton[4] used the modified quasichemical model for the Cu-Fe-S liquid solution with two different Gibbs energies for the copper-rich phase and a sulfur-rich molten phase. Waldner and Pelton[5] applied for the first time an improved version of the modified quasichemical model to a molten copper-sulfur and copper-iron-sulfur solution phase. Gibbs energy modeling for various Cu-S solid phases was carried out by Lee et al.[6] to assess the Cu-Fe-S system under consideration of an associate solution model specifically for the Cu-Fe-S liquid phase. Shishin et al.[7] performed a thermodynamic assessment of slag-matte-metal equilibria in the Cu-Fe-O-S-Si system based on a critical assessment and thermodynamic modeling of the Cu-Fe-S system by Waldner and Pelton[5] and of the Cu-O and Cu-O-S systems by Shishin and Decterov.[8] Jantzen et al.[9] applied the modified associate non-ideal solution approach with Cu_2S and FeS as liquid solution constituents for their Cu-Fe-S liquid phase model.

The aim of the present study is the prediction of sulfur potentials of the ternary Cu-Fe-S liquid solution applying the modified quasichemical model (MQM) solely on the basis of optimization studies of the binary subsystems Fe-

✉ Peter Waldner
peter.waldner@unileoben.ac.at

[1] Department of General, Analytical and Physical Chemistry, University of Leoben, Leoben, Austria

496

J. Phase Equilib. Diffus. (2022) 43:495–510

S,[10] Cu-S,[11,12] and Cu-Fe[13] without the use of ternary parameters. Despite different internal structures of the liquid phase ranging from metallic over matte-like to pure liquid sulfur solutions the mathematical description should be cast in one single Gibbs energy expression. Two different options for the excess Gibbs energy offered by MQM are compared with respect to its predictive ability for the Cu-Fe-S liquid solution. In order to calculate phase equilibria of the liquid solution with solid alloy phases and high-temperature pyrrhotite their Gibbs energies are modelled using the compound energy formalism. All experimental data available in the literature on sulfur potential data of the Cu-Fe-S liquid solution and on its high-temperature phase equilibria related to extended ternary miscibility gaps as well as to solid-state Cu-Fe-S phases should be considered for comparison with computations.

2 Experimental Data from the Literature

The sequence of the following quotations of experimental data from the literature within the subsequent sections for data on thermodynamic properties and phase equilibria of the Cu-Fe-S liquid phase is based on a chronological order.

2.1 Thermodynamic Data

Krivsky and Schuhmann[14] measured sulfur activities as a function of phase composition using $H_2S(g)/H_2(g)$ gas ratios in equilibrium with various Cu-Fe-S mixtures in the temperature range from 1150 °C (1423 K) to 1350 °C (1623 K). A thermogravimetric technique for continuous quantitative sulfur analysis of copper-iron-sulfur samples equilibrated with H_2S/H_2 gas mixtures was applied by Bale and Toguri.[15] Sulfur partial pressures together with liquid phase equilibria data of the Cu-Fe-S system were published for 1200 °C (1473 K). The measurement of sulfur potentials of Cu-Fe-S systems at 1250 °C (1523 K) was performed by Koh and Yazawa[16] equilibrating liquid matte with gaseous mixtures of H_2 and H_2S. Nagamori et al.[17] measured the vapor pressure of sulfur over Cu-Fe-S mattes by equilibrating them under H_2S-H_2 gas mixtures at 1200 °C (1473 K). Sulfur contents were determined gravimetrically as $BaSO_4$, while the metals iron and copper were analyzed by atomic absorption or titration technique.

2.2 Phase Diagram Data

Reuleaux[18] studied equilibria reactions of the partial system bounded within the Cu-Cu$_2$S-FeS-Fe composition tetragon applying thermal analysis, metallography (polished samples for optical microscopy) and chemical analysis. A comprehensive experimental study on Cu-Fe-S phase equilibria within the partial system Cu-Cu$_2$S-CuFeS$_2$-FeS$_{1.08}$-Fe was reported by Schlegel and Schüller[19] carrying out thermal analysis and microscopy with polarized reflected light. About 150 synthetic melting samples were investigated by X-ray diffraction.

Phase equilibria data not determined directly but derived from measurements of thermodynamic sulfur potentials by Krivsky and Schuhmann,[14] Bale and Toguri,[15] Koh and Yazawa,[16] and Nagamori et al.,[17] are also taken into account in this study. As these publications were already treated in the preceding section no further details are given here.

Ebel and Naldrett[20] investigated fractional crystallization of sulfide (Fe, Ni, Cu, S) ore liquids quenching them from temperatures between 1050 °C (1323 K) and 1180 °C (1453 K). Silica tube techniques were applied for more than 80 compositions of which the nickel-free ones are considered in this study. The phase relations in the miscibility gaps of the Cu-Fe-S-As and Cu-Fe-S-Sb systems with arsenic and antimony as minor elements were studied at 1200 °C (1473 K) by Mendoza et al.[21,22] using the quenching method. Data for tie-lines of arsenic- and antimony-free samples are reported for equilibria between the molten copper-rich metal and matte phases at 1200 °C (1473 K). Starykh et al.[23] used differential thermal analysis, scanning electron microscopy, and electron-probe microanalysis to study phase transformations involving the liquidus and solidus of the ternary Cu-Fe-S system. Data for the position of the miscibility gap boundary of the Cu-Fe-S system are given.

3 Thermodynamic Modeling

This study is focused on modeling Gibbs energies of the Cu-Fe-S liquid and all solid phases which are relevant for liquid–solid phase equilibria at elevated temperatures. Due to the complexity and large amount of experimental data of the Cu-Fe-S system, a study should be dedicated to the reporting on modeling results on low-temperature phase equilibria. The thermodynamic software package FactSage[24] specifically useful for treating systems with complex solution phases served as computation tool in this work. Standard Gibbs energy functions for Cu, Fe and S are taken from the Scientific Group Thermodata Europe (SGTE) unary database for pure elements, compiled by Dinsdale.[25] Table 1 lists all excess Gibbs energy parameters and model quantities treated in the subsequent sections for the liquid, pyrrhotite and alloy phases.

Table 1 Excess Gibbs energy parameters (in J mol^{-1}) and model quantities of the liquid, bcc, fcc and pyrrhotite phase according to binary optimization studies by Waldner and Pelton,[10] Waldner,[11,12] and Ansara and Janson,[13] as well as from this work

Phase: Liquid			
$\Delta g^o_{FeS} = -104{,}888.10 + 0.338\ T$			Ref. [10]
$g^{10}_{FeS} = +35{,}043.32 - 9.880\ T$			Ref. [10]
$g^{20}_{FeS} = +23{,}972.27$			Ref. [10]
$g^{30}_{FeS} = +30{,}436.82$			Ref. [10]
$g^{01}_{FeS} = +8626.26$			Ref. [10]
$g^{02}_{FeS} = +72{,}954.29 - 26.178\ T$			Ref. [10]
$g^{04}_{FeS} = +25{,}106$			Ref. [10]
$\Delta g^o_{CuS} = -62{,}467.12 - 11.071\ T$			Ref. [12]
$g^{10}_{CuS} = +45{,}905.22$			Ref. [12]
$g^{20}_{CuS} = -14{,}509.55$			Ref. [12]
$g^{01}_{CuS} = +9652.05$			Ref. [12]
$g^{02}_{CuS} = +33{,}890.40 - 15.188\ T$			Ref. [12]
$g^{04}_{CuS} = +33{,}205.00$			Ref. [12]
$^0L_{CuFe} = +36{,}088.00 - 2.32968\ T$			Ref. [13]
$^1L_{CuFe} = +324.53 - 0.03270\ T$			Ref. [13]
$^2L_{CuFe} = +10{,}355.40 - 3.60297\ T$			Ref. [13]
Phase: bcc alloy			
$^0L_{(Cu,Fe)} = 39{,}258.0 - 4.14983\ T$			Ref. [13]
$L_{(Fe,S)} = -31{,}041.003 - 10.657\ T$			Ref. [10]
Phase: fcc alloy			
$^0L_{(Cu,Fe)} = 48{,}232.5 - 8.60954\ T$			Ref. [13]
$^1L_{(Cu,Fe)} = 8861.88 - 5.28975\ T$			Ref. [13]
$L_{(Fe,S)} = -59{,}070.736 - 34.612\ T$			Ref. [10]
$L_{(Cu,S)} = -60{,}482.945 - 38.424\ T$			Ref. [11]

Model Compound	$\Delta_f H_{298.15}$ / kJ mol^{-1}	$S_{298.15}$ / J (K mol)$^{-1}$	
Phase: High-temperature Pyrrhotite			
$(Fe)_1(S)_1$	-96.291	69.429	Ref. [10]
$(Va)_1(S)_1$	$+140.049$	32.054	Ref. [10]
$(Cu)_1(S)_1$	-47.739	68.207	This work
$L_{(Fe,Va:S)} = 225{,}830.67 - 26.259\ T$	Ref. [10]		
$L_{(Fe,Cu:S)} = -39{,}748.00$	This work		

3.1 The Cu-Fe-S Liquid Solution

Two of the three subsystems show strong short-range ordering in the liquid state within a narrow composition range. This is the case at around 1/2 mol fraction of sulfur in the Fe-S system [10] and at around 1/3 mol fraction of sulfur in the Cu-S system.[12] Naturally, short-range ordering plays also a dominant role within the ternary Cu-Fe-S liquid solution. As a consequence, a thermodynamic model for the ternary melt over the entire composition range from purely metallic to pure liquid sulfur solutions should be able to merge properly short-range ordering

emanating even asymmetrically from both metal-sulfur systems.

In this study the total Gibbs energy of the ternary liquid phase as a function of temperature and composition according to

$$G = \left(n_{Cu}g^o_{Cu} + n_{Fe}g^o_{Fe} + n_S g^o_S\right) - T\Delta S^{config} + G^{ex}$$

(Eq 1)

is predicted based on previous optimizations of the binary subsystems Fe-S,[10] Cu-S,[12] and Cu-Fe[13] using the one-sublattice modified quasichemical model for multicomponent solutions by Pelton et al.[26] and Pelton and Chartrand.[27]

The term within the brackets of Eq 1 contains the molar Gibbs energies g_{Cu}^o, g_{Fe}^o and g_S^o of the pure components weighted with the numbers of moles of copper, iron and sulfur denoted with n_{Cu}, n_{Fe} and n_S. The product of the temperature T and the configurational entropy ΔS^{config} considers the energetic contribution due to random mixing of the (Cu-Cu), (Fe-Fe), (S-S), (Cu-S), (Fe-S), and (Cu-Fe) pairs in the one-dimensional Ising approximation:[26,27]

$$
\begin{aligned}
\Delta S^{config} = & -R(n_{Cu}\ln X_{Cu} + n_{Fe}\ln X_{Fe} + n_S\ln X_S) \\
& - R[n_{CuCu}\ln(X_{CuCu}/Y_{Cu}^2) \\
& + n_{FeFe}\ln(X_{FeFe}/Y_{Fe}^2) + n_{SS}\ln(X_{SS}/Y_S^2)] \\
& - R[n_{CuS}\ln(X_{CuS}/2Y_{Cu}Y_S,) \\
& + n_{FeS}\ln(X_{FeS}/2Y_{Fe},Y_S,) + n_{CuFe}\ln(X_{CuFe}/2Y_{Cu}Y_{Fe})]
\end{aligned}
$$

(Eq 2)

The mole fractions X_i and the coordination equivalent fractions Y_i are defined according to

$$X_i = n_i/(n_{Cu} + n_{Fe} + n_S) \tag{Eq 3}$$

$$Y_i = Z_i n_i/(Z_{Cu}n_{Cu} + Z_{Fe}n_{Fe} + Z_S n_S) \tag{Eq 4}$$

with the coordination numbers Z_i where $i = $ Cu, Fe and S. The pair fraction X_{ij} is given by the ratio number of moles of the (i-j) pairs n_{ij} divided by the total number of moles of all occurring pairs with i, j = Cu, Fe and S according to

$$X_{ij} = n_{ij}/(n_{CuCu} + n_{FeFe} + n_{SS} + n_{CuS} + n_{FeS} + n_{CuFe}) \tag{Eq 5}$$

The coordination numbers of copper, iron and sulfur can vary with composition as follows:

$$Z_{Cu} = (2n_{CuCu} + n_{CuS} + n_{CuFe})\left(\frac{2n_{CuCu}}{Z_{CuCu}^{Cu}} + \frac{n_{CuS}}{Z_{CuS}^{Cu}} + \frac{n_{CuFe}}{Z_{CuFe}^{Cu}}\right)^{-1} \tag{Eq 6}$$

$$Z_{Fe} = (2n_{FeFe} + n_{FeS} + n_{CuFe})\left(\frac{2n_{FeFe}}{Z_{FeFe}^{Fe}} + \frac{n_{FeS}}{Z_{FeS}^{Fe}} + \frac{n_{CuFe}}{Z_{CuFe}^{Fe}}\right)^{-1} \tag{Eq 7}$$

$$Z_S = (2n_{SS} + n_{FeS} + n_{CuS})\left(\frac{2n_{SS}}{Z_{SS}^S} + \frac{n_{FeS}}{Z_{FeS}^S} + \frac{n_{CuS}}{Z_{CuS}^S}\right)^{-1} \tag{Eq 8}$$

where Z_{CuCu}^{Cu} stands for the coordination number of copper when all nearest neighbors of copper are exclusively copper atoms, Z_{CuS}^{Cu} represents the quantity when all nearest neighbors are sulfur atoms and Z_{CuFe}^{Cu} when all nearest neighbors are iron atoms. The other coordination numbers in Eq 7 and 8 are defined in the same way when iron and sulfur are the central atoms within their corresponding neighborhood. The assessment of these quantities is treated in detail in the metal-sulfur binary studies[10,12] from which

numerical values are taken for this work: A value of 6.0 for the unary coordination numbers Z_{CuCu}^{Cu}, Z_{FeFe}^{Fe}, Z_{SS}^S, and the binary coordination numbers Z_{CuFe}^{Cu} and Z_{CuFe}^{Fe}, the values 1.5 and 3.0 for the binary coordination numbers Z_{CuS}^{Cu} and Z_{CuS}^S, respectively, and a value of 2.0 for Z_{FeS}^{Fe} and Z_{FeS}^S.

3.1.1 Excess Gibbs Energy of the Liquid Solution

The Gibbs energy function for the Cu-Fe-S liquid solution is based on a one-sublattice approach within the framework of the modified quasichemical model. Consequently first-nearest-neighbors' interactions between copper, iron and sulfur can be considered. The third term of Eq 1, the total excess Gibbs energy G^{ex}, summarizes the three types of first nearest-neighbors' interactions in the ternary solution phase:

$$G^{ex} = G_{CuS}^{ex} + G_{FeS}^{ex} + G_{CuFe}^{ex} \tag{Eq 9}$$

The quantity G_{CuS}^{ex} of Eq 9 stands for the first nearest-neighbors interaction between copper and sulfur species expressed by the following pair exchange reaction:

$$(Cu - Cu) + (S - S) = 2(Cu - S) \tag{Eq 10}$$
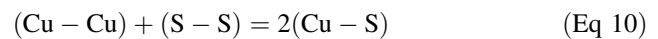
The non-configurational Gibbs energy change for the formation of two moles of (Cu-S) pairs according to reaction (10) is Δg_{CuS} which occurs in the excess term of the total Gibbs-energy:

$$G_{CuS}^{ex} = (n_{CuS}/2)\Delta g_{CuS} \tag{Eq 11}$$

The model quantity Δg_{CuS} determines on which side the equilibrium of reaction (10) is displaced. Its composition dependence exclusively based on binary interaction parameters can be expressed according to Pelton and Chartrand[27] through a polynomial expansion in terms of pair fractions:

$$\Delta g_{CuS} = \Delta g_{CuS}^o + \sum_{i \geq 1} g_{CuS}^{io} X_{SS}^i + \sum_{j \geq 1} g_{CuS}^{oj}(X_{CuCu} + X_{CuFe} + X_{FeFe})^j \tag{Eq 12}$$

Equation 12 reduces to the excess Gibbs energy of the Cu-S binary system when no iron is present and consequently X_{CuFe} and X_{FeFe} are zero. The adjustable, and in case of necessity temperature dependent parameters Δg_{CuS}^o, g_{CuS}^{io} and g_{CuS}^{oj} were optimized in the thermodynamic modeling study of the Cu-S liquid phase [12]. The superscripts noted as a ring, i and j identify the parameters given in the study of Waldner[12] as follows: The parameter Δg_{CuS}^o contributes decidedly to the excess Gibbs energy in the composition region where (Cu-S) pairs are dominating. The parameter g_{CuS}^{io} was selected and optimized in the sulfur-rich region where the pair fraction of (S-S) significantly exceeds the pair fractions of (Cu-Cu) and (Cu-S)

whereas the parameter g_{CuS}^{oj} is useful in copper-rich regions where the pair fraction of (Cu-Cu) significantly exceeds the pair fractions of (S-S) and (Cu-S).

Equation 12 shows an 'asymmetric' mathematical treatment of the mole fraction of sulfur pairs (S-S) in contrast to the mole fraction of (Cu-Cu) pairs which are exponentiated by j together with X_{CuFe} and X_{FeFe}. This different weighting of the energy parameters g_{CuS}^{io} and g_{CuS}^{oj} by the pair fractions originates in the well-known concept of Toop[28] to consider a chemically different component (here sulfur) compared with the other two component (here the metallic components copper and iron) specifically in the Gibbs energy of the ternary solution.

Also used in this study, an alternative possibility to extrapolate from binary parameters into ternary systems was proposed by Pelton and Chartrand[27] via another polynomial expansion in terms of pair fractions:

$$\Delta g_{CuS} = \Delta g_{CuS}^{o} + \sum_{i \geq 1} g_{CuS}^{io} \left(\frac{X_{SS}}{X_{SS} + X_{CuS} + X_{CuCu}} \right)^{i}$$
$$+ \sum_{j \geq 1} g_{CuS}^{oj} \left(\frac{X_{CuCu}}{X_{SS} + X_{CuS} + X_{CuCu}} \right)^{j}$$

$$(Eq\ 13)$$

Equation 13 reduces also to the excess Gibbs energy of the Cu-S binary system when the iron content is zero. Again, the parameters Δg_{CuS}^{o}, g_{CuS}^{io} and g_{CuS}^{oj} are taken from the thermodynamic modeling study of the Cu-S liquid phase.[12] The mathematically 'symmetric' weighting of the energy parameters g_{CuS}^{io} and g_{CuS}^{oj} by pair fraction terms originates from the well-known concept of Kohler[29] where at constant ratios of e.g. the two system components copper and sulfur a constant contribution of Cu-S interaction energies is taken into account in the Gibbs energy equation of the ternary system.

Within a ternary system the 'chemical asymmetry' of one system component according to Toop[28] and the 'energetic symmetry' of two system components according to Kohler[29] are reflected geometrically in Gibbs triangle representations and induce classifications in terms of so called geometric solution models.[30,31]

The second term of Eq 9, G_{FeS}^{ex}, is related to the other type of first nearest-neighbors interaction between iron and sulfur species according to the pair exchange reaction:

$$(Fe - Fe) + (S - S) = 2(Fe - S) \qquad (Eq\ 14)$$
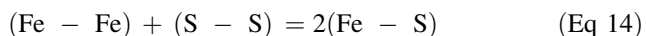
Like the Cu-S liquid phase following equation can be noted for the contribution of the Fe-S liquid phase to the excess Gibbs energy:

$$G_{FeS}^{ex} = (n_{FeS}/2)\Delta g_{FeS} \qquad (Eq\ 15)$$

The composition dependency of Δg_{FeS} is formulated in an analogous manner as described for Δg_{CuS} containing corresponding parameters Δg_{FeS}^{o}, g_{FeS}^{io} and g_{FeS}^{oj} either according to Eq 12 or 13. The optimized values of the parameters Δg_{FeS}^{o}, g_{FeS}^{io} and g_{FeS}^{oj} are given in the thermodynamic modeling study of the Fe-S system.[10]

Finally, the first-nearest-neighbors interaction between the two metallic species copper and iron is considered by the quantity

$$G_{CuFe}^{ex} = (n_{CuFe}/2)\Delta g_{CuFe} \qquad (Eq\ 16)$$

The modified quasichemical model also permits the integration of binary subsystems optimized with a random-mixing Bragg-Williams and Redlich–Kister model. Following expression for the composition dependency of Δg_{CuFe} is given according to Pelton and Chartrand[27] for a 'symmetric' consideration of copper and iron analogous to Kohler:[29]

$$\Delta g_{CuFe} = \sum_{i \geq 0} \frac{1}{3} {}^{i}L_{CuFe} \left(\frac{Y_{Cu} - Y_{Fe}}{Y_{Cu} + Y_{Fe}} \right)^{i} \qquad (Eq\ 17)$$

In the Cu-Fe binary subsystem the Eq 16 together with Eq 17 reduces to a 'Redlich–Kister' expression for which the adjustable model parameters ${}^{i}L_{CuFe}$ were taken from Ansara and Jansson.[13] The factor 1/3 originates from the term $2/Z_{CuFe}^{Cu} = 2/Z_{CuFe}^{Fe} = 2/6$ which is necessary to transform the parameters ${}^{i}L_{CuFe}$ into the parameter Δg_{CuFe} according to the definition of a pair exchange reaction within the modified quasichemical model by Pelton et al.[26]

3.2 High-Temperature Pyrrhotite

Binary high-temperature pyrrhotite is the dominating solid state phase in the Fe-S subsystem exhibiting a crystal structure of the $B8_1$-type (Pearson symbol hP4, space group $P6_3/mmc$, NiAs prototype). No equivalent phase exists in the Cu-S subsystem.[11] Nevertheless, ternary phase diagram data, as will be shown in the next section, indicate a limited solubility of copper in high-temperature pyrrhotite emanating from the Fe-S subsystem.[10] The notation $(Fe)_{1-x}S$ reflects possible deviation from stoichiometry by formation of vacancies on the octahedral metal sublattice in the NiAs prototype structure. The sulfur atoms occupy a hexagonally closed-packed (hcp) substructure. Since the high-temperature pyrrhotite phase $Fe_{1-x}S$ is successfully described by a two-sublattice model according to $(Fe,Va)_1(S)_1$ where Va stands for possible vacancies[10] copper solubility is considered according to $(Cu,Fe,Va)_1(S)_1$ where the first sublattice models the octahedral positions for the metal atoms and the vacancies (Va). The

500

J. Phase Equilib. Diffus. (2022) 43:495–510

second sublattice represents the close-packed hexagonal array of sulfur atoms. The compound energy formalism provides following analytical expression for the molar Gibbs energy according to the two-sublattice approach $(Cu,Fe,Va)_1(S)_1$:

$$G_m = \left(y_{Fe}G^o_{FeS} + y_{Cu}G^o_{CuS} + y_{Va}G^o_{VaS}\right) \\ + RT\left(y_{Fe} \ln y_{Fe} + y_{Cu} \ln y_{Cu} + y_{Va} \ln y_{Va}\right) + G^{ex}_m$$

(Eq 18)

The compound energy formalism derived by Hillert and Staffansson,[32] and generalized by Sundman and Ågren[33] defines three compound energies in Eq 18 as model quantities. The quantities G^o_{FeS} and G^o_{CuS} are the molar Gibbs energies of defect-free stoichiometric FeS and CuS, respectively. G^o_{VaS} is the molar Gibbs energy of hypothetical sulfur with pyrrhotite structure. The site fractions of iron, copper, and vacancies on the metal sublattice are denoted with y_{Fe}, y_{Cu} and y_{Va}, respectively. G^o_{FeS} and G^o_{VaS} are accepted from the study [10], G^o_{CuS} stands for hypothetical CuS with pyrrhotite structure and is estimated using the heat capacity and absolute third law molar entropy at 25 °C (298.15 K) of covelite CuS [11]. The enthalpy of formation at 25 °C (298.15 K), $\Delta_f H_{298.15}$, is optimized in this study with – 47,739 kJ mol^{-1}.

The molar excess Gibbs energy expression G^{ex}_m consists of two expressions where the first one originates from the binary model for high-temperature iron pyrrhotite.

$$G^{ex}_m = y_{Fe}y_{Va} L_{(Fe,Va:S)} + y_{Fe}y_{Cu} L_{(Fe,Cu:S)}$$

(Eq 19)

The second expression accounts for the copper-iron interaction which is assessed in this study with the adjustable model quantity $L_{(Fe,Cu:S)}$ = – 39,748 J/mol. The data for $L_{(Fe,Va:S)}$ are taken from the previous study[10] on binary high-temperature iron pyrrhotite.

3.3 Solid Metallic Phases

Two solid alloy solutions with body-centered (bcc) and face-centered (fcc) cubic structure are involved in phase equilibria with the ternary liquid solution at elevated temperatures. The Gibbs energies of both alloy phases are taken from Ansara and Jansson[13] where the mutual solubility of the metal atoms was described by a substitutional approach. In this study the same approach is accepted for the thermodynamic description of the limited sulfur solubility in iron and copper provided by Waldner and Pelton[10] and by Waldner,[11] respectively. Following molar Gibbs energy function can be noted commonly for both alloy solutions:

$$G_m = \left(x_{Fe}G^o_{Fe} + x_{Cu}G^o_{Cu} + x_S G^o_S\right) + RT(x_{Fe} \ln x_{Fe} \\ + x_{Cu} \ln x_{Cu} + x_S \ln x_S) + G^{ex}_m$$

(Eq 20)

The quantities G^o_{Fe} and G^o_{Cu} are the standard molar Gibbs energies of the pure solid metals and are taken from Dinsdale.[25] The standard molar Gibbs energy G^o_S refers to hypothetical pure sulfur within the metallic structures. The first nearest neighbor interaction energies between the three solution constituents iron, copper and sulfur are considered by the molar excess Gibbs energy G^{ex}_m which can be expanded according to a Redlich–Kister polynomial as a function of temperature and composition:

$$G^{ex}_m = x_{Cu}x_{Fe} \sum_{n \geq 0} {}^n L_{(Cu,Fe)}(x_{Cu} - x_{Fe})^n + x_S x_{Fe} L_{(Fe,S)} \\ + x_S x_{Cu} L_{(Cu,S)}$$

(Eq 21)

# 4 Comparison of Prediction with Experimental Data

As the liquid solution dominates the high-temperature Cu-Fe-S system the extrapolation scheme from the binary subsystems into the ternary system is apart from the binaries optimizations also crucial for the predictive ability of the used Gibbs energy model. Experimental data on sulfur potentials and phase equilibria available in the literature for elevated temperatures are compared with prediction results.

4.1 Asymmetric versus Symmetric Model Approach for G^{ex} of the Cu-Fe-S Liquid Solution

The choice of Eq 12 for Δg_{CuS} and of the analogous one for Δg_{FeS} as well as of Eq 17 for Δg_{CuFe} results in an excess Gibbs energy G^{ex} in Eq 9 which is noted in this study as asymmetric model approach. In contrast to the asymmetric model approach the symmetric alternative uses Eq 13 for Δg_{CuS} and the analogous one for Δg_{FeS} instead of Eq 12 for excess Gibbs energy G^{ex} in Eq 9. Together with Eq 17 for Δg_{CuFe} three symmetric contributions are forming an excess Gibbs energy which is noted in this study as symmetric model approach. Calculations are undertaken using the same optimization results for the binary subsystems. Thus, the influence of the choice for the asymmetric model approach on the prediction of sulfur potentials and phase equilibria can be compared with the results according to the symmetric model approach.

At this stage the demonstration of prediction results is oriented to sulfur potentials and phase equilibria exemplarily for 1200 °C (1473 K). To show the predicted sulfur potentials and the stability of the liquid phase over the entire composition range gas phase formation at higher sulfur content is suppressed. Thereby possible demixing

Fig. 1 Asymmetric (solid lines) vs. symmetric (dotted lines) model approach: Predicted sulfur potentials (expressed as equilibrium pressure of S_2) of the Cu-Fe-S liquid solution at two ternary ratios n_{Fe} / ($n_{Fe} + n_{Cu}$) for 1200 °C (1473 K) together with experimental data (ratio numbers given after symbols)
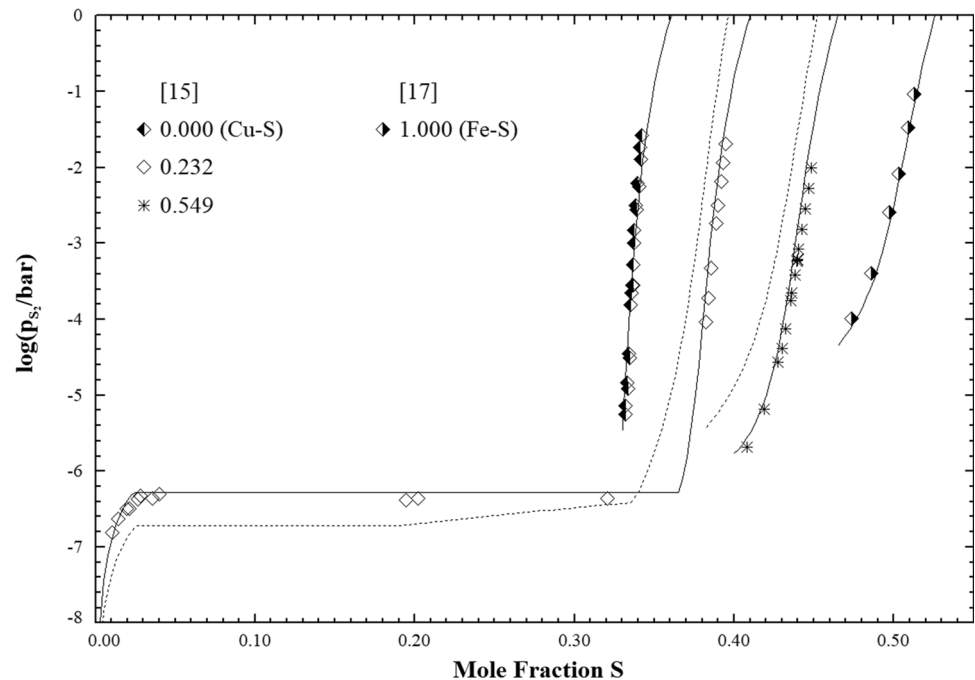
behavior is made visible in metastable sulfur-rich regions. Since test calculations at 1150 °C (1423 K) and 1350 °C (1623 K) give analogous results the findings of the present section are seen as valid for other temperatures.

Figure 1 presents the obtained predictions which are compared with selected but representative experimental data of sulfur potentials at 1200 °C (1473 K) from Bale and Toguri[15] and Nagamori et al.[17] All other experimental data available from the literature will be treated in the subsequent chapter in Fig. 3. Experimental sulfur potentials at 1200 °C (1473 K) are expressed as equilibrium pressures of S_2 gas in Fig. 1. Using the thermodynamically ideal description of the gas phase species as $S_n(g)$ from $S_1(g)$ to $S_8(g)$ as well as Cu(g), $Cu_2(g)$, CuS(g) and $Cu_2S(g)$ are taken into consideration. Standard Gibbs energy functions of these gaseous species are taken from the SGTE pure substance database. Two data sets at the ratios n_{Fe} / ($n_{Fe} + n_{Cu}$) = 0.232 and 0.549 are shown for comparison with the model predictions given as solid lines according to the asymmetric approach and as dotted lines according to the symmetric approach. Naturally the computations for the subsystems Cu-S and Fe-S remain unchanged since the same binary interaction parameters are involved.

The predictions of the liquid phase model using the asymmetric approach are in satisfactory agreement with experimental data in the composition range between 1/3 (Cu-S edge) and 1/2 (Fe-S edge) mole fraction of sulfur where the sulfur potentials show a strong change over several orders of magnitude.

Figure 1 contains also experimental data points[15] for the ratio n_{Fe} / ($n_{Fe} + n_{Cu}$) = 0.232 at lower mole fraction of sulfur around 0.03 up to 0.32 which are related to a two- and three- phase region. Within the two-phase region a metallic copper-rich liquid phase coexists with an iron-rich fcc (face-centered cubic) alloy phase. The three-phase regime, represented as horizontal line in Fig. 1, is a miscibility gap between metallic and sulfur-rich liquids in equilibrium with an iron-rich fcc alloy phase. Agreement of the predicted line for the ratio n_{Fe} / ($n_{Fe} + n_{Cu}$) = 0.232 with experimental data ranges from fair to very satisfactory. Substantial deviations of model prediction from experimental data are observed when the symmetric model approach is used.

Furthermore, the symmetric model approach is analyzed by equilibria calculations to map all predicted phase relations at 1200 °C (1473 K). The obtained isothermal section is shown in Fig. 2(a). It differs substantially from the prediction using the asymmetrical model approach which is treated in Fig. 8 with all experimental data available from the literature in the subsequent chapter together with other isothermal sections at 1150 °C (1423 K), 1250 °C (1523 K) and 1350 °C (1623 K). The above stated failure to reproduce sulfur potential data within the three-phase region Liq(1) + Liq(2) + fcc is reflected by the fact that the Cu-Fe matte corner of the corresponding tie-line triangle (denoted in Fig. 2(a) with A) is shifted to too high iron and low sulfur contents. This corner is part of the phase boundary limiting the extended one-phase region 'Liquid' towards the metal-rich part of the system. This phase boundary is not in line with the experimental

data.[15,17] In addition complex phase relations close to the binary subsystems are predicted which are denoted in Fig. 2(a) as equilibria C and D and as equilibria E and F very close to the Fe-S and Cu-S system, respectively. However, the expansion of these four equilibria regimes is so small that they are not visible in Fig. 2(a). Moreover, several two-phase regions and even phase regimes with three liquid phases are computed at higher sulfur contents. As a result, several kinks occur on the phase boundary of Fig. 2(a) separating the single matte phase field from the

extended region of immiscibility between matte and an almost pure liquid sulfur solution. It can be concluded that on one hand the symmetric model approach predicts a too high stability of the matte at lower sulfur contents and on the other hand a too low stability towards sulfur-rich regions. This mismatch can also be clearly seen in Fig. 1 concerning the computed sulfur potential for the ratio $n_{Fe} / (n_{Fe} + n_{Cu}) = 0.232$. At lower mole fraction of sulfur, the calculation falls below the experimental data whereas in the composition range of short range ordering (between

Fig. 2 (a) Symmetric model approach: Predicted isothermal section of the Cu-Fe-S phase diagram at 1200 °C (1473 K) together with experimental data. Predicted phase boundaries are shown as solid lines, predicted tie-lines as dashed lines and experimental tie-lines as solid lines. Abbreviation: fcc stands for face-centered cubic alloy phase, here iron-rich. (b) Molar Gibbs energies of the liquid solution predicted according to the asymmetric (solid lines) vs. symmetric (dotted lines) model approach along the Cu-FeS$_{1.02}$ join at molar Fe/S ratio of 1/1.02. (c) Molar Gibbs energies of the liquid solution predicted according to the asymmetric (solid lines) vs. symmetric (dotted lines) model approach along the Fe-Cu$_5$FeS$_4$ join at molar Cu/S ratio of 5/4. (d) Molar Gibbs energies of the liquid solution predicted according to the asymmetric (solid lines) vs. symmetric (dotted lines) model approach at mass Fe/Cu ratio of 55/45
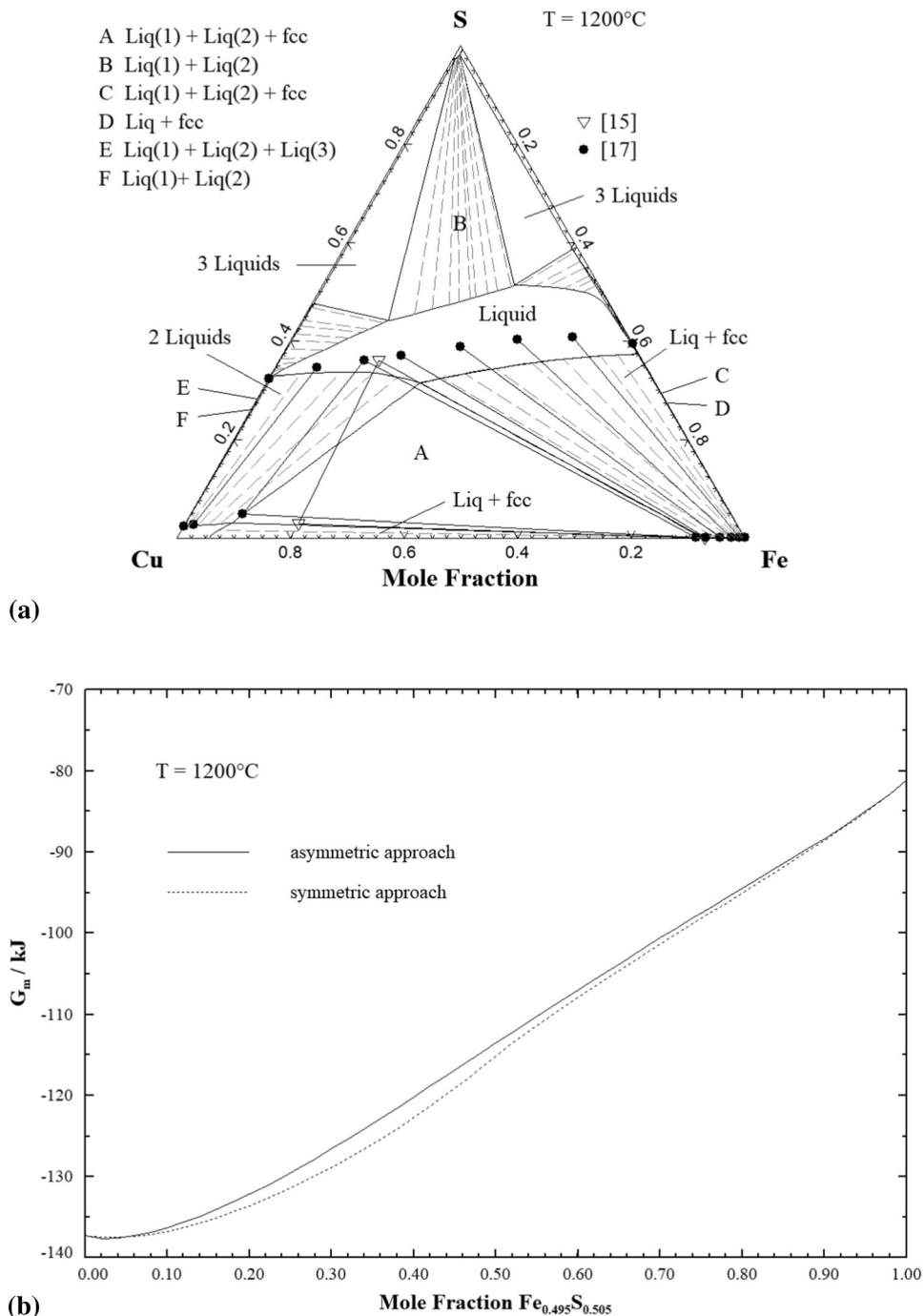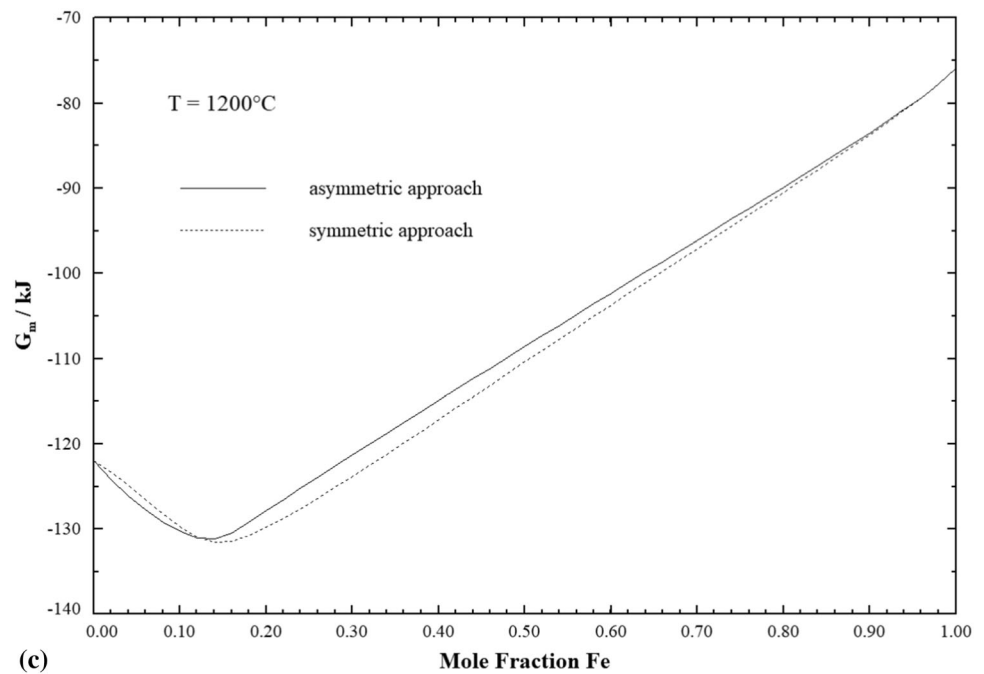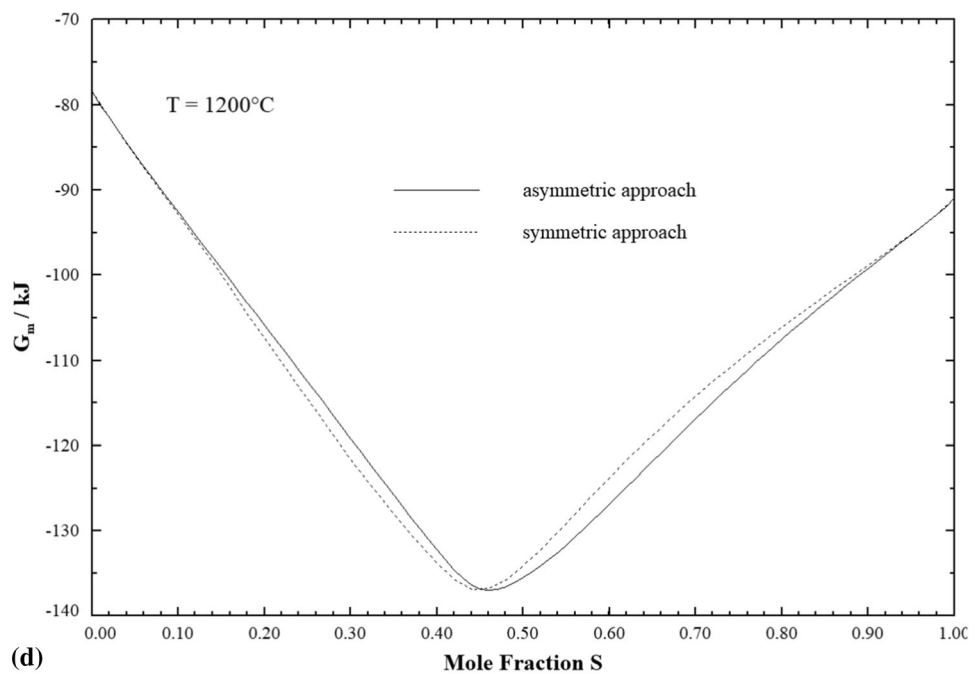
J. Phase Equilib. Diffus. (2022) 43:495–510

503

Fig. 2 continued

(c)

(d)

around 1/3 and 1/2 mol fraction of sulfur) sulfur potentials are predicted too high.

In order to illustrate the predictive behavior shown in Fig. 2(a) from a more fundamental point of view Gibbs energies of the liquid solution predicted according to the asymmetric or symmetric model approach are shown in the Fig. 2(b), (c) and (d): Computations are performed at 1200 °C (1473 K) along three isoplethal sections which correspond to Fig. 11 (Cu-FeS$_{1.02}$ join at molar Fe/S ratio of 1/1.02), Fig. 12 (Fe-Cu$_5$FeS$_4$ join at molar Cu/S ratio of 5/4) and Fig. 13 (at mass Fe/Cu ratio of 55/45) and which are treated in the subsequent chapter. The predicted Gibbs energies show clear differences concerning their minima and curvature behavior which are crucial for common tangents in thermodynamic equilibria relations.

Fig. 3 Predicted sulfur potentials (expressed as equilibrium pressure of S_2) of the Cu-Fe-S liquid solution together with experimental data. The values next to each symbol stand for a certain ratio n_{Fe} / $(n_{Fe} + n_{Cu})$
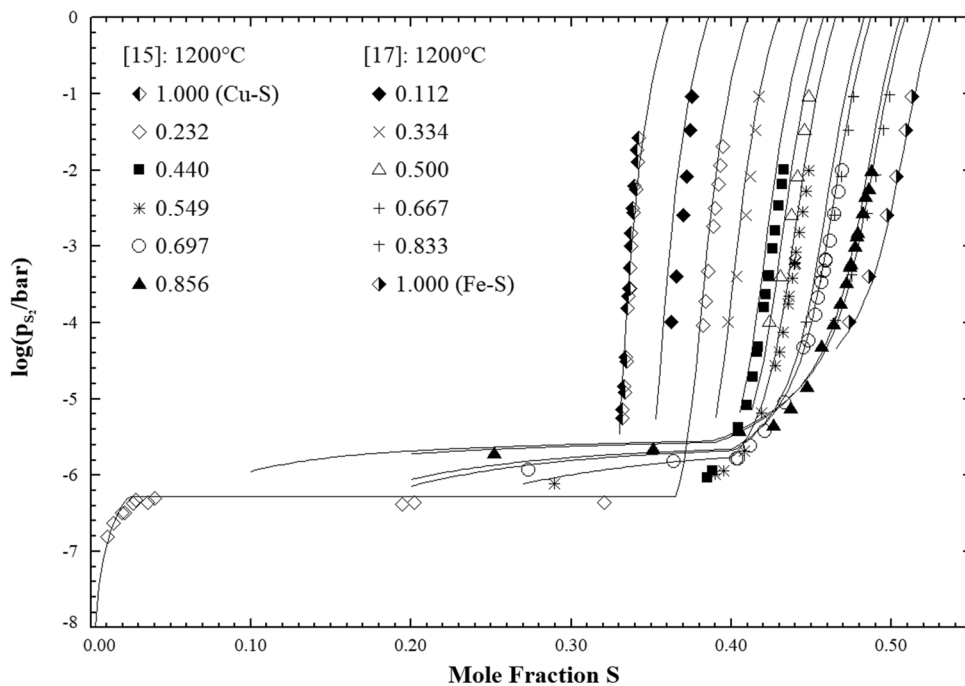
Fig. 4 Predicted sulfur potentials (expressed as equilibrium pressure of S_2) of the Cu-Fe-S liquid solution together with experimental data. The values next to each symbol stand for a certain ratio n_{Fe} / $(n_{Fe} + n_{Cu})$
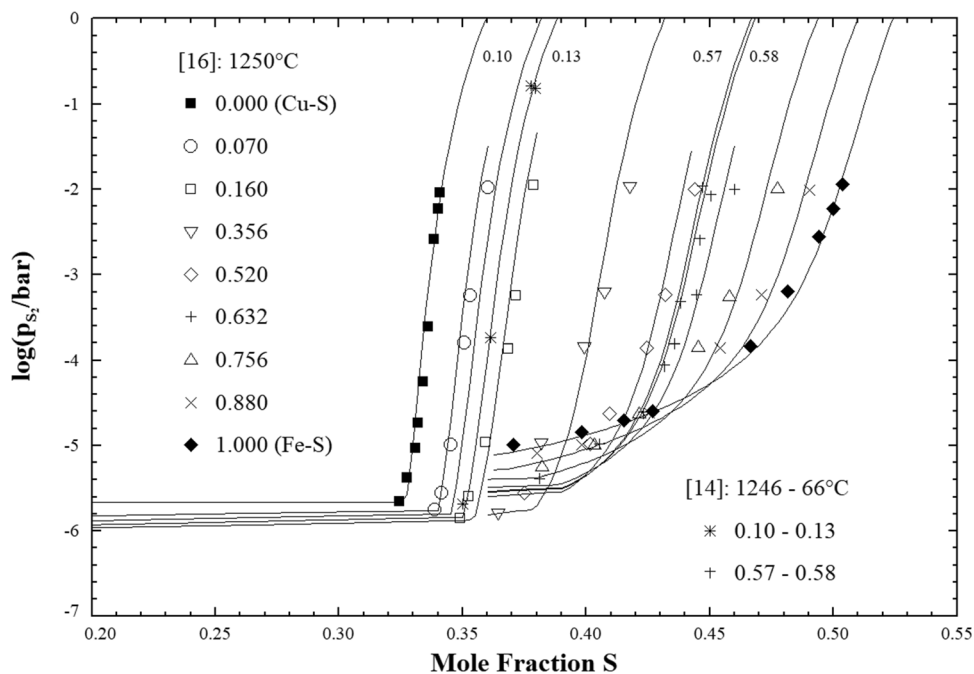
4.2 Prediction of Sulfur Potentials

A clear difference in predictive ability between asymmetric versus symmetric model approach is demonstrated in favor of the first one in the preceding section. Consequently, the asymmetric model approach is used for the Gibbs energy of the Cu-Fe-S liquid solution to carry out predictive computations of sulfur potentials and phase equilibria.

At first the predictive ability is studied with respect of experimental data such as sulfur potentials which are exclusively related to the liquid phase and no Gibbs energy model of other phases is involved. Figures 3, 4, 5 and 6 give a comprehensive survey of all experimental sulfur potential data available in the literature, expressed as equilibrium pressures of S_2 gas between around 1150 °C (1423 K) and 1350 °C (1623 K). In Fig. 3 and 4 experimental data[14–17] are shown which cover at 1200 °C
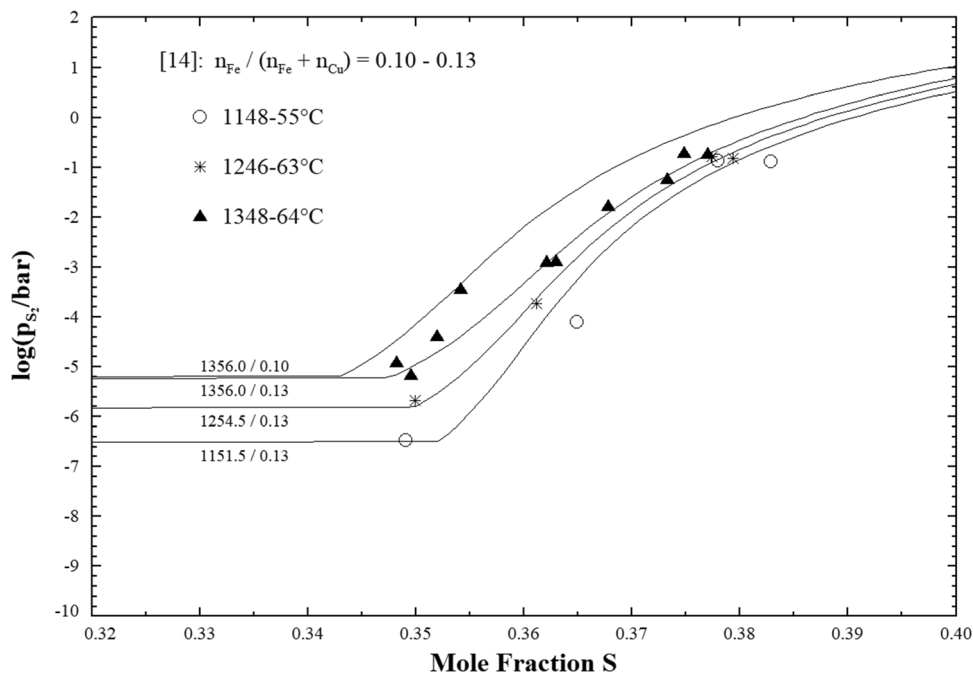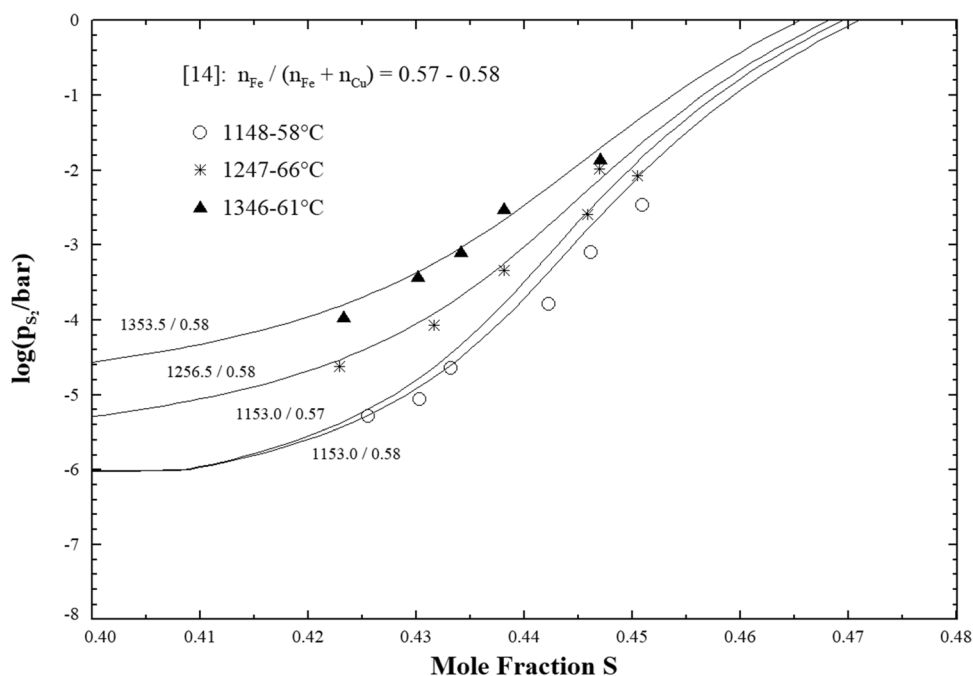
Fig. 5 Predicted sulfur potentials (expressed as equilibrium pressure of S_2) of the Cu-Fe-S liquid solution at a certain ratio n_{Fe} / ($n_{Fe} + n_{Cu}$) together with experimental data

Fig. 6 Predicted sulfur potentials (expressed as equilibrium pressure of S_2) of the Cu-Fe-S liquid solution at a certain ratio n_{Fe} / ($n_{Fe} + n_{Cu}$) together with experimental data

(1473 K) and 1250 °C (1523 K) the composition range from the Cu-S binary through increasing ratios n_{Fe} / ($n_{Fe} + n_{Cu}$) up to the Fe-S binary edge. The liquid phase model of this study can predict (depicted as solid lines) satisfactorily a large amount of experimental data in the composition range between 1/3 (Cu-S edge) and 0.5 (Fe-S edge) mole fraction of sulfur where the sulfur potentials show a strong change over several orders of magnitude. As already discussed with Fig. 1 data also

related to two and three-phase regions can be predicted satisfactorily (see ratio n_{Fe} / ($n_{Fe} + n_{Cu}$) = 0.232). Figure 5 and 6 demonstrate experimental sulfur potentials [14] between around 1150 °C (1423 K) and 1350 °C (1623 K) for two narrow ranges of the ratios n_{Fe} / ($n_{Fe} + n_{Cu}$). To estimate the sensitivity of the model prediction the calculation for 1356 °C (1629 K) – 1356 is with 1/2 (1348 + 1364) the arithmetic mean of the temperature range given by Krivsky and Schuhmann[14]—is performed
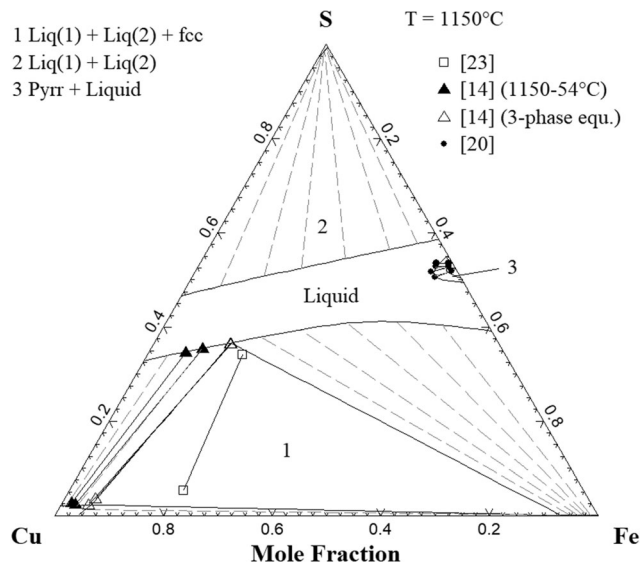
Fig. 7 Predicted isothermal section at 1150 °C (1423 K) of the Cu-Fe-S phase diagram together with experimental data. Experimental tie-lines are shown as solid lines; calculated tie-lines are shown as dashed lines. Abbreviation: fcc stands for the face-centered-cubic Cu-Fe-alloy phase, Pyrr for high-temperature Fe-Cu-pyrrhotite
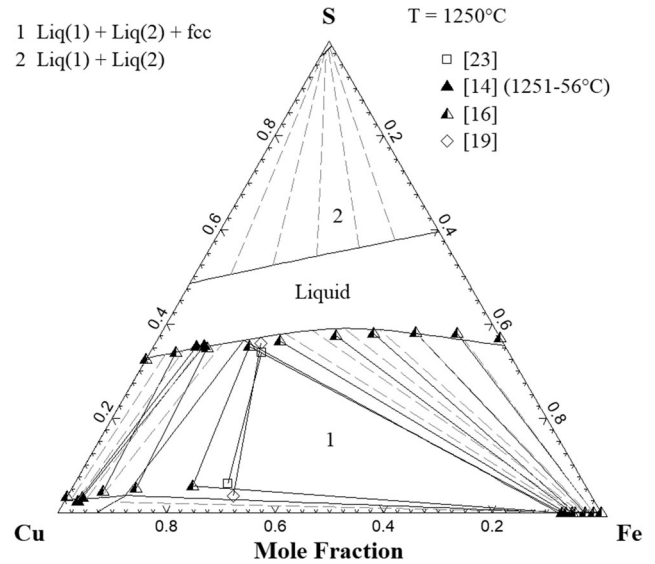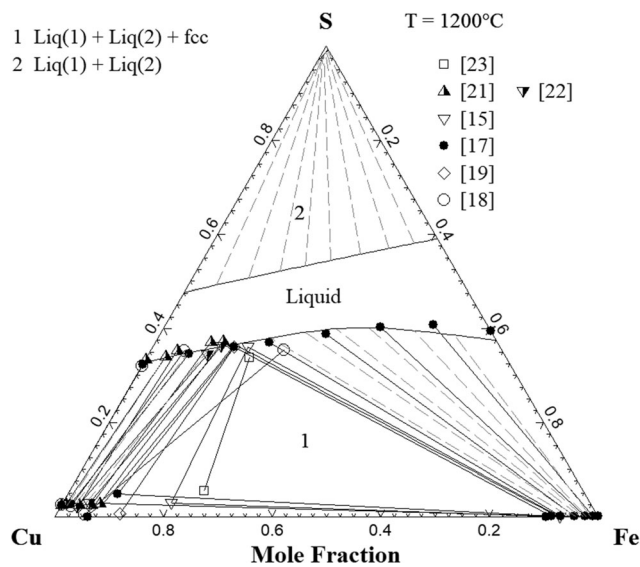

Fig. 9 Predicted isothermal section at 1250 °C (1523 K) of the Cu-Fe-S phase diagram together with experimental data. Experimental tie-lines are shown as solid lines; calculated tie-lines are shown as dashed lines. Abbreviation: fcc stands for the face-centered-cubic Cu-Fe-alloy phase
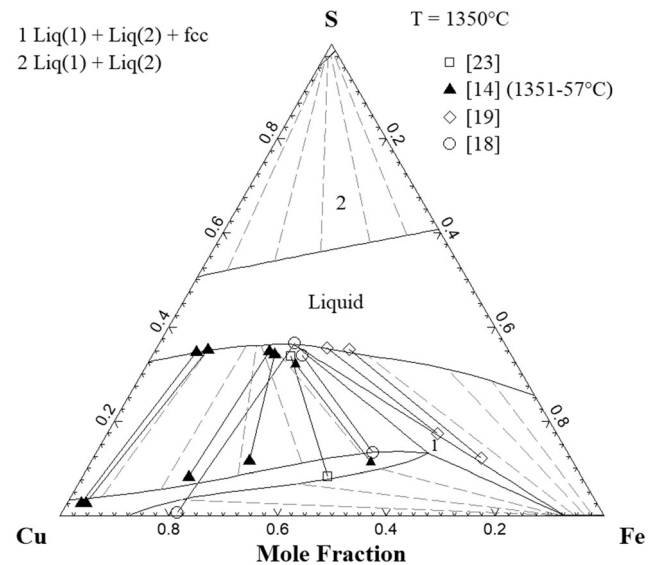

Fig. 8 Predicted isothermal section at 1200 °C (1473 K) of the Cu-Fe-S phase diagram together with experimental data. Experimental tie-lines are shown as solid lines; calculated tie-lines are shown as dashed lines. Abbreviation: fcc stands for the face-centered-cubic Cu-Fe-alloy phase

Fig. 10 Predicted isothermal section at 1350 °C (1623 K) of the Cu-Fe-S phase diagram together with experimental data. Experimental tie-lines are shown as solid lines; calculated tie-lines are shown as dashed lines. Abbreviation: fcc stands for the face-centered-cubic Cu-Fe-alloy phase

4.3 Prediction of Phase Equilibria–Isotherms

Isothermal sections at four distinct temperatures are shown over the entire composition range in the Fig. 7, 8, 9 and 10. The four temperatures are chosen at 1150 °C, 1200 °C, 1250 °C, and 1350 °C (1423 K, 1473 K, 1523 K, and 1623 K) according to the availability of experimental data

in Fig. 5 for both end points 0.10 and 0.13 of the reported range of the ratios $n_{Fe}/(n_{Fe} + n_{Cu})$. The analogous is done in Fig. 6 for the model prediction for both end points 0.57 and 0.58 of the reported range of the ratios $n_{Fe}/(n_{Fe} + n_{Cu})$. The model prediction shows reasonable agreement with most of the experimental data given in the Fig. 5 and 6.

from the literature.[14–23] Experimentally determined tie-lines are plotted as solid lines where the two end points are indicated by a certain symbol. Predicted tie-lines in two-phase regions are shown as dashed lines. The region of immiscible liquid solutions emanating from the Cu-S edge is predicted in line with the experimental data at all four temperatures. In contrast to Fig. 2(a) the phase boundary limiting the extended one-phase region 'Liquid' towards the metal-rich part of the system is in line with experimental data as Fig. 8 and 9 show over the entire composition range up to the Fe-S edge. At 1150 °C (1423 K) the experimental tie-line triangle of the three-phase equilibrium Liq(1) + Liq(2) + fcc (denoted with 1 in Fig. 7) can be reproduced very well by the prediction. At 1200 °C (1473 K) the corresponding experimental tie-line triangle of the three-phase equilibrium Liq(1) + Liq(2) + fcc by Nagamori et al.[17] and two tie-lines of the corresponding triangle by Bale and Toguri[15] are also well predicted. A significant deviation of the experimental (as well as the predicted) copper-rich corner of Nagamori et al.[17] from the experimental one of Bale and Toguri[15] can be seen. As demonstrated in the Fig. 1 and 3 there is good agreement between calculation and experimental data according to the ratio $n_{Fe} / (n_{Fe} + n_{Cu}) = 0.232$ of which the long horizontal line is directly related to the three-phase equilibria Liq(1) + Liq(2) + fcc and therefore to the corresponding tie-line triangle in Fig. 4. Therefore, above deviation may be interpreted as inconsistency of the cooper–rich corner of the triangle of Bale and Toguri[15] with their own sulfur

potential data shown in the Fig. 1 and 3 as well as with the data of Nagamori et al.[17] The data from Starykh et al.[23] except for the highest temperature at 1350 °C (1623 K) are neither in line with other experimental data nor can be reproduced by the calculations. At the lowest temperature of the four isothermal sections, high-temperature pyrrhotite is the only solid sulfide that is stable. The isothermal section at 1150 °C (1423 K) shows a two-phase region Pyrr + Liquid (denoted with 3 in Fig. 7) where the phase field of high-temperature pyrrhotite emanates from the Fe-S subsystem due to limited solubility of copper.

In general, the majority of predicted phase boundaries agrees satisfactorily with experimental data shown in the four isothermal sections.

4.4 Prediction of Phase Equilibria–Isopleths

The Fig. 11, 12, 13 and 14 show four predicted isoplethal sections together with experimental phase diagram data.[14–23] The four isopleths cut through the Cu-Cu$_2$S-FeS-Fe regime such that a wide composition range of the high-temperature Cu-Fe-S system is covered. Figure 11 represents the Cu-FeS join (the exact chosen stoichiometry Fe$_{0.495}$S$_{0.505}$ of the mole fraction-axis originates from the fact, that Schlegel and Schüller[19] have put FeS$_{1.02}$ as endpoint of their drawn isopleth; confer also the congruent melting-point of high-temperature Fe-pyrrhotite which is not exactly at the Fe$_1$S$_1$ stoichiometry[10]). On the other hand, Fig. 12 corresponds to the Fe-Cu$_5$FeS$_4$ join which

Fig. 11 Predicted isoplethal section (solid lines) at molar Fe/S ratio of 1/1.02 along the Cu-FeS$_{1.02}$ join of the Cu-Fe-S phase diagram together with experimental data
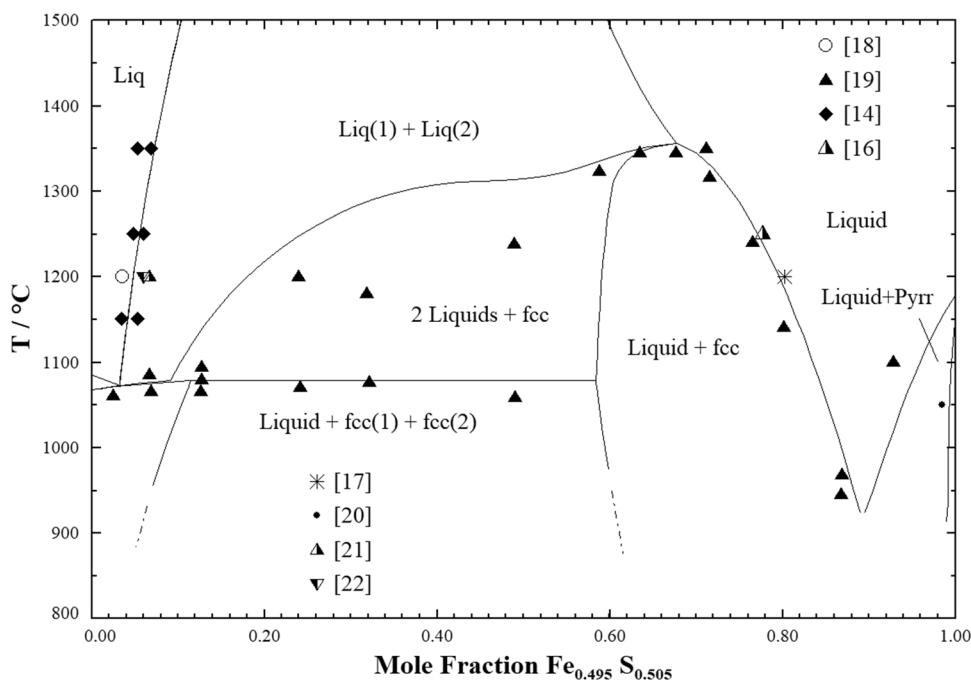
Fig. 12 Predicted isoplethal section (solid lines) at molar Cu/S ratio of 5/4 along the Fe-Cu₅FeS₄ join of the Cu-Fe-S phase diagram together with experimental data
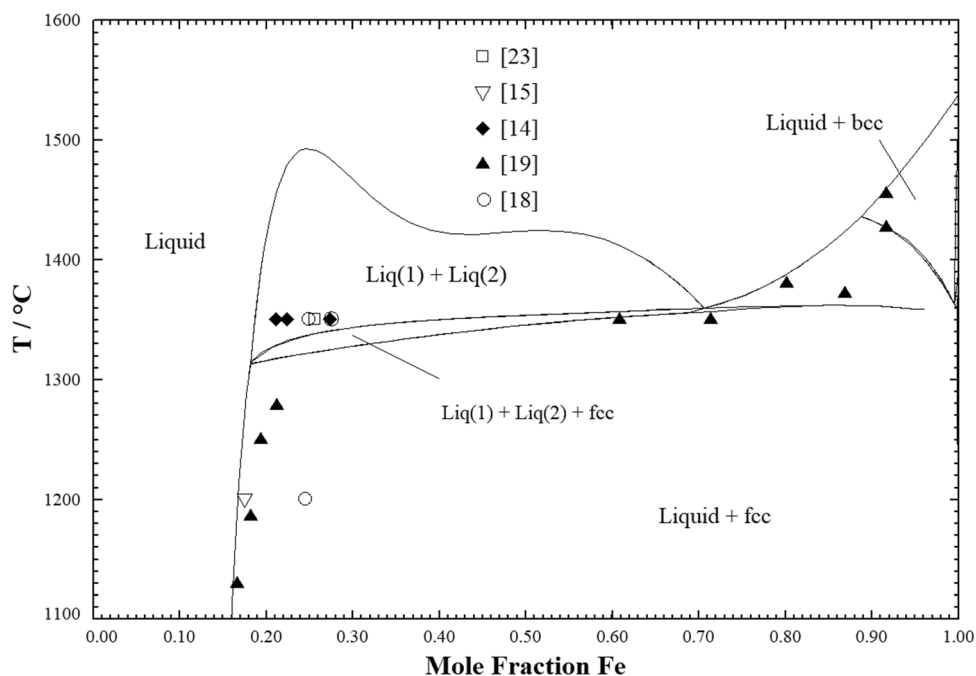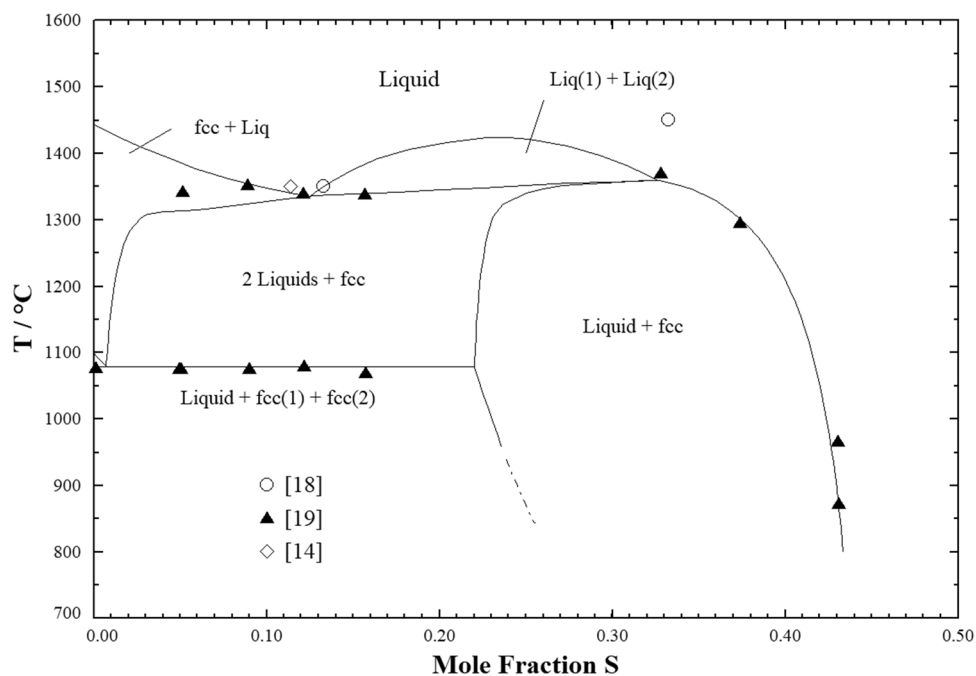

Fig. 13 Predicted isoplethal section (solid lines) at mass Fe/Cu ratio of 55/45 of the Cu-Fe-S phase diagram together with experimental data


crosses the system starting from the Fe-corner. Alternatively, Fig. 13 starts in the S-corner to terminate in the Cu-Fe subsystem at a mass Fe/Cu ratio of 55/45. Finally, the isopleth of Fig. 14 is calculated at 82 wt.-% Fe.

All isoplethal sections show that the predicted phase boundaries (solid lines) agree reasonably with the majority of experimental data points related to e.g. the ternary miscibility gap (regions denoted with Liq(1) + Liq(2)) and

phase fields where the alloy phases (fcc, bcc) and high-temperature pyrrhotite are involved. Agreement between the predicted four-phase equilibrium Liq(1) + Liq(2) + fcc(1) + fcc(2) around 1080 °C (1353 K) shown in the Fig. 5, 7 and 14 with experimental data is very satisfactory.

J. Phase Equilib. Diffus. (2022) 43:495–510

509

Fig. 14 Predicted isoplethal section (solid lines) at 82 wt.-% Fe of the Cu-Fe-S phase diagram together with experimental data
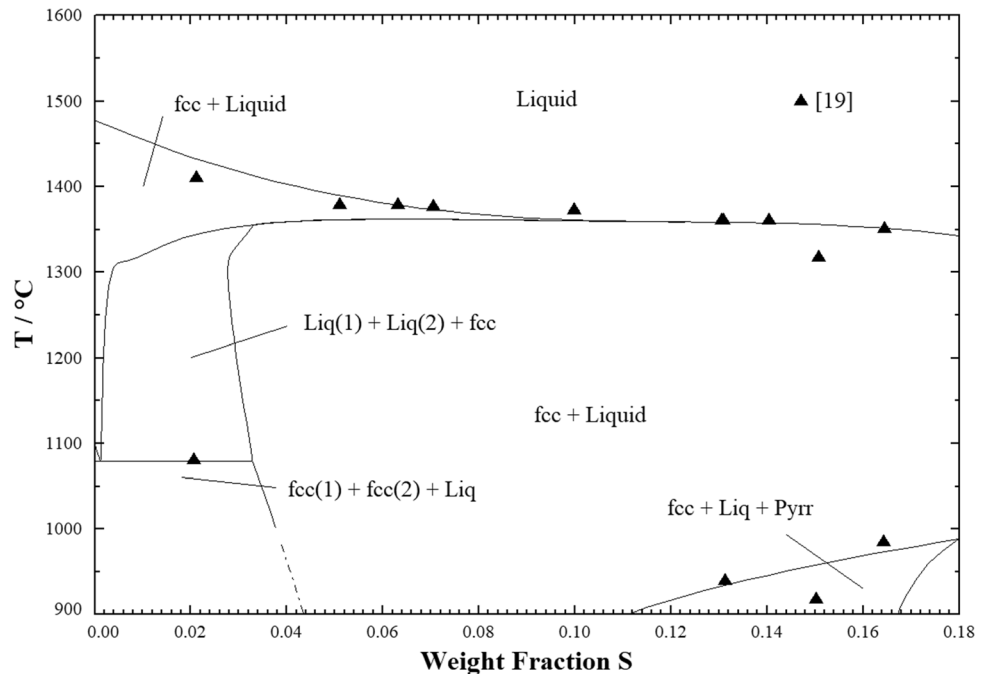
5 Conclusions

Within the framework of the modified quasichemical model an asymmetric model approach for the excess Gibbs energy allows satisfactory predictions of sulfur potentials of the Cu-Fe-S liquid solution solely on the basis of previous Cu-S, Fe-S and Cu-Fe optimizations. It is feasible to use one single Gibbs energy function over the entire composition range although the chemistry of the Cu-Fe-S liquid solution varies strongly from metallic to pure liquid sulfur. Limited copper solubility is taken into consideration by extension the two-sublattice model for high-temperature pyrrhotite using the compound energy formalism. Together with Cu-Fe-S alloy phases complex phase relations with the Cu-Fe-S liquid solution can be calculated in line with a large body of experimental data. Without the necessity of additional adjustable ternary parameters for the Gibbs energy of the Cu-Fe-S liquid solution the presented study may contribute to comprehensive thermodynamic multi-component/-phase databases for metal-sulfur systems and/or to integrated databases for metal-oxygen-sulfur systems.

Data Availability The data required to reproduce these findings are available within the article or cited in the reference list.

References

1. Y.A. Chang, Y.E. Lee, and J.P. Neumann, *Extractive Metallurgy of Copper*, J.C. Yannopoulos and J.C. Agrawal, ed., The Metallurgical Society AIME, New York, 1976, p 21–48.
2. Y.A. Chang, J.P. Neumann, and U.V. Choudray, Phase diagrams and thermodynamic properties of Cu-S-metal systems, in: INCRA Monograph VII, The Int. Copper Research Association, Inc., New York., 1979, p 58–88.
3. F. Kongoli, Y. Dessureault, and A.D. Pelton, Thermodynamic Modeling of Liquid Fe-Ni-Cu-Co-S Mattes, *Metall. Mater. Trans. B*, 1998, **29**, p 591–601.
4. S.A. Degterov, and A.D. Pelton, A Thermodynamic Database for Copper Smelting and Converting, *Metall. Mater. Trans. B*, 1999, **30**, p 661–669.
5. P. Waldner, and A.D. Pelton, Thermodynamic modeling of the Cu-Fe-S system, unpublished research, École Polytechnique de Montreal, Montreal, QC, Canada, 2006.

6. B.J. Lee, B. Sundman, S.I.I. Kim, and K.G. Chin, Thermodynamic Calculation on the Stability of Cu$_2$S in Low Carbon Steels, *ISIJ Int.*, 2007, **47**(1), p 163–171.

7. D. Shishin, E. Jak, and S.A. Decterov, Thermodynamic Assessment of Slag-Matte-Metal Equilibria in the Cu-Fe-O-S-Si System, *J. Phase Equilib. Diff.*, 2018, **39**, p 456–475.

8. D. Shishin, and S.A. Decterov, Critical Assessment and Thermodynamic Modeling of the Cu-O and Cu-O-S Systems, *Calphad*, 2012, **38**, p 59–70.

9. T. Jantzen, K. Hack, E. Yazhenskikh, and M. Mueller, Evaluation of Thermodynamic Data and Phase Equilibria in the System Ca-Cr-Cu-Fe-Mg-Mn-S Part II: Ternary and Quasi-ternary Subsystems, *Calphad*, 2017, **56**, p 286–302.

10. P. Waldner, and A.D. Pelton, Thermodynamic Modeling of the Fe-S System, *J. Phase Equilib. Diff.*, 2005, **26**, p 23–38.

11. P. Waldner, Solid-State Phase Equilibria of the Cu-S System: Thermodynamic Modeling, *J. Phase Equilib. Diff.*, 2018, **39**(6), p 810–819.

12. P. Waldner, Gibbs Energy Modeling of the Cu-S Liquid Phase: Completion of the Thermodynamic Calculation of the Cu-S System, *Metall. Mater. Trans. B*, 2020, **51**(2), p 805–816.

13. I. Ansara, and A. Jansson, System Cu-Fe, Thermochemical database for light metal alloys, in: I. Ansara, A.T. Dinsdale, M.H. Rand (Eds.), COST 507, 1998, p 165–167.

14. W.A. Krivsky and R. Schuhmann Jr., Thermodynamics of the Cu-Fe-S System at Matte Smelting Temperatures, *Trans. AIME*, 1957, **209**, p 981–988.

15. C.W. Bale, and J.M. Toguri, Thermodynamics of the Cu-S, Fe-S and Cu-Fe-S Systems, *Can. Metall. Quart.*, 1976, **15**(4), p 305–318.

16. J. Koh, and A. Yazawa, Thermodynamic Properties of the Cu-S, Fe-S and Cu-Fe-S Systems, *Bull. Res. Inst. Mineral Dress. Metall. Tohoku Univ. Sendai*, 1982, **38**(2), p 107–118.

17. M. Nagamori, T. Azakami, and A. Yazawa, Activities in the Cu-Fe-S Mattes at 1473 K, *Metall. Rev. MMIJ*, 1989, **6**(2), p 112–127.

18. O. Reuleaux, Reaktionen und Gleichgewichte im System Cu-Fe-S mit besonderer Berücksichtigung des Kupfersteins, *Metall. Erz*, 1927, **24**(5), p 99–111. (**in German**)

19. H. Schlegel, and A. Schüller, Das Zustandsbild Kupfer-Eisen-Schwefel, *Freib. Forschungsh.*, 1952, **B**(2), p 1–32. (**in German**)

20. D.S. Ebel and A.J. Naldrett, Fractional Crystallization of Sulfide Ore Liquids at High Temperature, *Econ. Geol.*, 1996, **91**, p 607–621.

21. D.G. Mendoza, M. Hino, and K. Itagaki, Phase Relations and Aktivity of Arsenic in Cu-Fe-S-As System at 1473 K, *Mater. Trans.*, 2001, **42**(11), p 2427–2433.

22. D.G. Mendoza, M. Hino, and K. Itagaki, Phase Relations and Aktivity of Antimony in Cu-Fe-S-Sb System at 1473 K, *Mater. Trans.*, 2002, **42**(5), p 1166–1172.

23. R.V. Starykh, S.I. Sineva, and S.B. Zakhryapin, Study of the Liquidus and Solidus Surface in the Quaternary Fe-Ni-Cu-S System: IV. Construction of a Meltability Diagram and Determination of Miscibility Gap Boundaries for the Ternary Cu-Fe-S Sulfide System, *Russ. Metall. (Met.)*, 2010, 2010 (11), p 1025–1031.

24. C.W. Bale, E. Bélisle, P. Chartrand, S.A. Decterov, G. Eriksson, A.E. Gheribi, K. Hack, I.-H. Jung, Y.-B. Kang, J. Melançon, A.D. Pelton, S. Petersen, C. Robelin, J. Sangster, P. Spencer, and M.-A. VanEnde, FactSage Thermochemical Software and Databases, 2010–2016, *Calphad*, 2016, **54**, p 35–53.

25. A.T. Dinsdale, SGTE Data for Pure Elements, *Calphad*, 1991, **15**(4), p 317–425.

26. A.D. Pelton, S.A. Degterov, G. Eriksson, C. Robelin, and Y. Dessureault, The Modified Quasichemical Model I - Binary Solutions, *Metall. Trans. B*, 2000, **31**, p 651–659.

27. A.D. Pelton and P. Chartrand, The Modied Quasi-Chemical Model: Part II. Multicomponent Solutions, *Metall. Trans. A*, 2001, 32, p 1355–1360.

28. G.W. Toop, Predicting Ternary Activites Using Binary Data, *Trans. AIME*, 1965, **232**, p 850–855.

29. F. Kohler, Zur Berechnung der thermodynamischen Daten eines ternären Systems aus den zugehörigen binären Systemen, *Monatsh. Chemie*, 1960, **91**(4), p 738–740. (**in German**)

30. M. Hillert, Empirical methods of predicting and representing thermodynamic properties of ternary solution phases, *Calphad*, 1980, **4**(1), p 1–12.

31. A.D. Pelton, A general 'geometric' thermodynamic model for multicomponent solutions, *Calphad*, 2001, **25**(2), p 319–328.

32. M. Hillert and L.I. Staffanson, Regular Solution Model for Stoichiometric Phases and Ionic Melts, *Acta Chem. Scand.*, 1970, **24**(10), p 3618–3626.

33. B. Sundman and J. Ågren, A Regular Solution Model for Phases with Several Components and Sublattices, Suitable for Computer Applications, *J. Phys. Chem. Solids*, 1981, **42**(4), p 297–301.